LIMNOLOGY
and
OCEANOGRAPHY

ASLO

Limnol. Oceanogr. 9999, 2019, 1–13

doi: 10.1002/lno.11327

Vertical stratification and stability of biogeochemical processes in the deep saline waters of Lake Vanda, Antarctica

Charles A. Schutte [1,a] **Vladimir A. Samarkin,** [1,†] **Brian Peters,** [2] **Michael T. Madigan,** [3] **Marshall Bowles,** [4] **Rachael Morgan-Kiss,** [5] **Karen Casciotti,** [2] **Samantha Joye** [1*]

[1]Department of Marine Sciences, University of Georgia, Athens, Georgia
[2]Department of Earth System Science, Stanford University, Stanford, California
[3]Department of Microbiology, Southern Illinois University, Carbondale, Illinois
[4]Louisiana Universities Marine Consortium (LUMCON), Chauvin, Louisiana
[5]Department of Microbiology, Miami University, Oxford, Ohio

Abstract

Lake Vanda is a permanently ice-covered lake in the McMurdo Dry Valleys of Antarctica. Its bottom waters remain stratified year-round because of a strong salinity-driven density gradient. We have assessed spatial patterns in and relationships between major biogeochemical processes in the water column of Lake Vanda. Samples were collected in the austral summers of 2008 and 2011 to measure concentrations of metabolites associated with a suite of biogeochemical processes across the deep salinity gradient. The shapes of the resulting geochemical profiles were consistent between 2008 and 2011. Metabolite production and consumption rates were estimated using a reactive transport model based on the assumption that vertical diffusion was the only active physical transport process. We validated this model for nitrification by using stable isotope incubations to show that this process was only active at depths predicted by the model. No nitrification activity was observed at 68 m depth in spite of overlapping oxygen and ammonium gradients. We attribute this lack of activity to the competitive inhibition of ammonia monooxygenase by methane. Net nitrous oxide and nitrate consumption were observed in the oxic water column, providing evidence of aerobic denitrification. The depth of maximum net oxygen production did not coincide with the deep chlorophyll maxima (at 59.3, 63, and 68.2 m) measured in the same profile. Finally, the integrated sulfide oxidation rate was high compared with other oxidation processes, indicating that sulfide was an important electron donor for the water column microbial community.

The lakes of the McMurdo Dry Valleys in Antarctica are natural laboratories for microbiologists and biogeochemists for at least three reasons: (1) they are remote and relatively uninfluenced by human activity; (2) their physical and chemical stratification is very stable, resulting in a microbial community with a predictable vertical structure; and (3) they are extreme environments for microorganisms due to their low temperature and high salinity. Lake Vanda is located within the Wright Valley and has been studied extensively since the 1960s. Lake Vanda is a closed-basin, permanently ice-covered, meromictic (i.e., no seasonal turnover of the water column) lake that receives glacial meltwater supplied by the Onyx River, the longest river in Antarctica. Like many of the Dry Valleys lakes, Lake Vanda has no outlet: water gain from the Onyx River is balanced by ablation of surface ice. In the past two decades, warmer summers have contributed to a significant lake level rise (Castendyk et al. 2016).

The upper water column (above ~ 55 m) of Lake Vanda is cold, fresh, oxic, and well mixed by convection (Ragotzkie and Likens 1964). This freshwater layer, which constitutes most of the lake's water column, overlies a dense calcium chloride brine that reaches a salinity of 124 PSU or higher, more than 3.5 times greater than seawater. This brine is the remnant of an ancient lake that was concentrated via evaporation into a brine pool during an extremely dry period approximately 1200 yr ago (Wilson 1964). When glacial meltwater began flowing again, it filled in the lake basin above the brine, creating a distinct halocline that separated the fresh and saline layers. The density of the underlying brine is sufficient to maintain stratification despite an inverted thermal gradient.

*Correspondence: mjoye@uga.edu

Additional Supporting Information may be found in the online version of this article.

[†]Deceased 14 February 2017

[a]Present address: Department of Environmental Science, Rowan University, Glassboro, New Jersey

Lake Vanda bottom waters are warmed by solar energy that is focused deep in the lake by the highly transparent surface ice (Tregoning et al. 2015).

The intense and stable salinity-driven density gradient ensures that diffusion is the only mass transport mechanism within the brine that makes up Lake Vanda bottom water (Canfield and Green 1993). When the temperature gradient is destabilizing the salinity-driven density gradient, it is possible that double diffusion can cause vertical mixing over depth ranges that are typically around 0.5–2 m (Schmid et al. 2010). Double-diffusive convection results in a characteristic "staircase" where multiple mixed layers are separated by steep temperature gradients. This phenomenon has been observed in Lake Kivu (Schmid et al. 2010) and Lake Nyos (Schmid et al. 2004). Hoare (1966) also showed that double diffusion occurs in the portion of the Lake Vanda water column where salinities first start to increase, over a conductivity range of $\sim$ 1.8–4.8 mS cm^{-1} ($\sim$ 1.4–3.8 PSU based on the assumption of seawater composition). However, temperature increased smoothly through the bulk of the deep brine in Lake Vanda (Hoare 1966), supporting diffusion-driven transport. Furthermore, Canfield and Green (1993) showed that ion ratios in the brine are consistent with diffusion-only transport. Therefore, diffusive fluxes can be calculated from the concentration gradients derived from depth profiles of any given solute in the deep brine. The upward or downward diffusive fluxes of a solute can be summed for any given depth interval, and the production or consumption rate required to mass balance the total flux estimated. This method for calculating rates is particularly useful in the Lake Vanda environment because rates are very low due to cold temperatures, hypersalinity, and low microbial cell densities (Canfield and Green 1993).

Previous studies of biogeochemical processes in Lake Vanda bottom waters revealed a typical vertical stratification along the salinity gradient, which starts $\sim$ 20 m above the lake bottom. Nitrification is active in the oxic waters at the top of the salinity gradient ($\sim$ 15 m above the lake bottom) and oxygenic photosynthesis is most active just a few meters deeper (Vincent and Downes 1981). Denitrification becomes active $\sim$ 8–10 m above the lake bottom (Vincent and Downes 1981) where the water becomes anoxic. Active metal cycling is focused around this oxic/anoxic interface (Bratina et al. 1998). In general, metal inputs from the Onyx River are oxidized in the oxygenated surface layers of the lake where they form particles and sink. When they reach the interface with anoxic deep waters, they are reduced and solubilized, creating a characteristic concentration peak (Green and Lyons 2009). Many metals (e.g., iron, manganese, copper, cadmium, nickel) form precipitates with sulfide in deeper waters and are buried in the sediment.

Many previous studies of biogeochemical processes in Lake Vanda have focused on one theme, such as nitrous oxide cycling (Vincent and Downes 1981; Peters et al. 2014), nutrient cycling (Canfield and Green 1993), or metal cycling (Bratina et al. 1998; Green and Lyons 2009). The goal of the present work was to estimate rates of a suite of carbon-, oxygen-, nitrogen-, sulfur-, and metal-cycling processes in order to understand their vertical stratification and identify relationships between them. This goal was pursued by measuring potential rates of microbial activity (e.g., nitrification), quantifying depth profiles of several key microbial substrates and metabolic byproducts, fitting these profiles with cubic spline interpolation functions, and calculating the second derivative of those functions for use in a reactive transport model to estimate net reaction rates. Briefly, our results show that the deep saline waters of Lake Vanda are highly stable with respect to their chemical and physical structure and also the diverse microbial processes they support. By simultaneously analyzing a broad suite of microbial metabolites, we were able to make connections between diverse biogeochemical processes and show, for example, that the integrated sulfide oxidation rate was high compared with other (e.g., ammonium and methane) oxidation processes, indicating that sulfide was an important electron donor for the water column microbial community.

Methods

Sample collection

Water column samples were collected from the deep western basin of Lake Vanda (77°32.0292′S 161°33.1674′E) on 07 December 2008 and 01 December 2011. A hole was drilled through the 3.0 m and 2.8 m of ice covering the lake surface in 2008 and 2011, respectively. A profiling spectrofluorometer (FluoroProbe, BBE Moldaenke GmbH, Germany) was lowered through the water column on a hand winch to determine chlorophyll *a* (Chl *a*) concentrations and relative abundance of major algal classes according to Dolhi et al. (2015). The FluoroProbe was corrected for yellow substances using an integrated colored dissolved organic matter correction factor on the instrument. While Fluoroprobe data were not verified using cell counts, they have been validated for the phytoplankton communities from the nearby Lake Fryxell and Lake Bonney (Dolhi et al. 2015), and chlorophyll maxima measured there agreed with those reported previously (Burnett et al. 2006). Abundances of four major spectral phytoplankton groups (green algae, cryptophytes, cyanobacteria, and a mixed group of diatoms and haptophytes) were estimated with the FluoroProbe based on their absorption characteristics of their light-harvesting antenna pigments (Beutler et al. 2002). In marine systems, the "mixed algae" class of the FluoroProbe is typically dominated by diatoms; however, previous reports have shown that diatoms are rare in Lake Vanda, and the mixed signal is likely associated with haptophytes in the water columns of the Dry Valley lakes (Bielewicz et al. 2011; Kong et al. 2012; Dolhi et al. 2015). This mixed group will therefore be referred to as "haptophytes" throughout this article. Photosynthetically available radiation (PAR) was measured with a Li-Cor LI-193 spherical quantum sensor (Li-Cor Biosciences, NE). Next, a 5-liter Niskin bottle was lowered successively

from 60 to 74 m depth at 2 m intervals using a hand winch. Immediately after each sample reached the surface, dissolved oxygen concentration (2011 only) and temperature were measured using a polarographic probe (Orion DO Probe for lab or field) and pH was measured using a separate electrode (Orion ROSS Sure Flow pH Electrode) connected with the same handheld meter (Thermo Fisher Orion 5-Star portable meter). An additional subsample of water was collected in a 1-liter polypropylene bottle and sealed with no headspace using a thick, butyl rubber stopper and returned to the laboratory at McMurdo for subsampling later the same day. Salinity was measured from this bottle using a handheld salinity meter (YSI Model 30) in practical salinity units (PSU), a unitless salinity scale that is based on the conductivity of seawater and is functionally equivalent to the salt concentration in parts per thousand ($g\ kg^{-1}$). The YSI Model 30 converts conductivity to salinity assuming seawater composition of salts. We measured a salinity range of 9–146 PSU in Lake Vanda brine, which is equivalent to a conductivity range of 11.1–160.2 $mS\ cm^{-1}$. Correcting these conductivities for a standard temperature of 25°C to facilitate comparison with other lakes yields a range of 14.4–171.1 $mS\ cm^{-1}$.

Chemical analyses

The protocols and procedures used in this study align with those described by Saxton et al. (2016). The two colorimetric analyses described below (ammonium and sulfide) were conducted within a week of sample collection. All other subsamples were shipped back to the laboratory in the United States for analysis. A 10-mL subsample was collected into a disposable syringe and injected into a 20-mL serum vial for trace gas (methane and nitrous oxide) analysis. The serum vial had been prepurged with helium and contained a sodium hydroxide pellet to halt metabolic activity; each vial was sealed with a butyl rubber septum and stored inverted. Methane concentrations were measured using a gas chromatograph (Shimadzu GC2100) equipped with a flame ionization detector. Nitrous oxide was measured on a separate injection of the same sample using a gas chromatograph (Shimadzu GC8A) fitted with a Hayesep DB column and electron capture detector. All other subsamples were first passed through a 0.2 μm syringe filter that was rinsed with 1 mL of sample to prevent sample oxidation or contamination. A 5-mL subsample for sulfide analysis was 0.2-μm filtered into a 15-mL centrifuge tube and fixed with 200 μL of 20% (w/v) zinc acetate and stored at 4°C until analysis using the Cline (1969) colorimetric method. A third 20-mL subsample was filtered into an acid-washed Nalgene bottle and stored frozen for nutrient and dissolved organic carbon (DOC) analysis. DOC and total dissolved nitrogen were measured by catalytic combustion using a Shimadzu TOC5000. Nitrite was measured using standard colorimetric methods (Bendschneider and Robinson 1952). Nitrate + nitrite was measured by vanadium reduction using an Antek 7050 chemiluminescent nitric oxide detector. Nitrate concentrations were calculated by difference between nitrate + nitrite and nitrite. A fourth 5-mL subsample was filtered into a 15-mL centrifuge tube containing 200 μL of phenol reagent and stored refrigerated until colorimetric analysis of ammonium (Solorzano 1969). Dissolved organic nitrogen was calculated as the difference between total dissolved nitrogen and the sum of ammonium, nitrate, and nitrite. A final 20-mL subsample was filtered into a glass scintillation vial and fixed with 0.05 mL of concentrated nitric acid. From this sample, concentrations of dissolved metals, including iron, manganese, nickel, copper, zinc, molybdenum, cadmium, barium, lead, and vanadium, were measured by inductively coupled plasma mass spectrometry (PerkinElmer ELAN DRC ICP-MS). Samples were measured against a multielement standard dissolved in 2% nitric acid (Environmental Express ACQ500-7). A yttrium internal standard (in 2% nitric acid; Environmental Express HP100067-1) was added to all samples and standards.

Net rate calculations

Net metabolite production and consumption rates were calculated over the 60–74 m depth range using a reactive transport model adapted from Berner (1980) under the simplifying assumptions that metabolite concentrations were at steady state and that the only physical process influencing their transport was diffusion. Double-diffusive convection likely influenced solute transport just below the freshwater/brine interface over a conductivity range of 1.8–4.8 $mS\ cm^{-1}$ (Hoare 1966). Comparing the shape of the temperature profile measured by Hoare (1966) with our own (Fig. 1a), this zone covered a depth range of $\sim$ 48–53 m. However, we applied this reactive transport model deeper in the brine (60–74 m) where conductivities were much higher (11.1–160.2 $mS\ cm^{-1}$) and there was no evidence for solute transport processes other than diffusion.

$$D\frac{\partial^2 C}{\partial z^2} + \sum R = 0 \quad (1)$$

Here, D is the diffusion coefficient ($m^2\ d^{-1}$), C is the metabolite concentration ($\mu mol\ m^{-3}$), z is the water depth (m), and $\sum R$ is the net reaction rate ($nmol\ L^{-1}\ d^{-1}$). To solve this equation, a natural cubic spline function was fit to each concentration profile and the second derivative of that function calculated using the splinefun function in the R stats package (Team 2017). Because of steep salinity and temperature gradients at the depths of interest, it was unrealistic to assume a constant diffusion coefficient. Diffusion coefficients across a range in temperatures from 0°C to 25°C for each metabolite were taken from Schulz and Zabel (2006), and a linear regression of diffusion coefficient as a function of temperature was fit to each to calculate the diffusion coefficient at any given temperature:

$$D_T = mD + b \quad (2)$$

where D is the diffusion coefficient at 0°C, D_T is the diffusion coefficient at temperature T, m is the slope of the linear

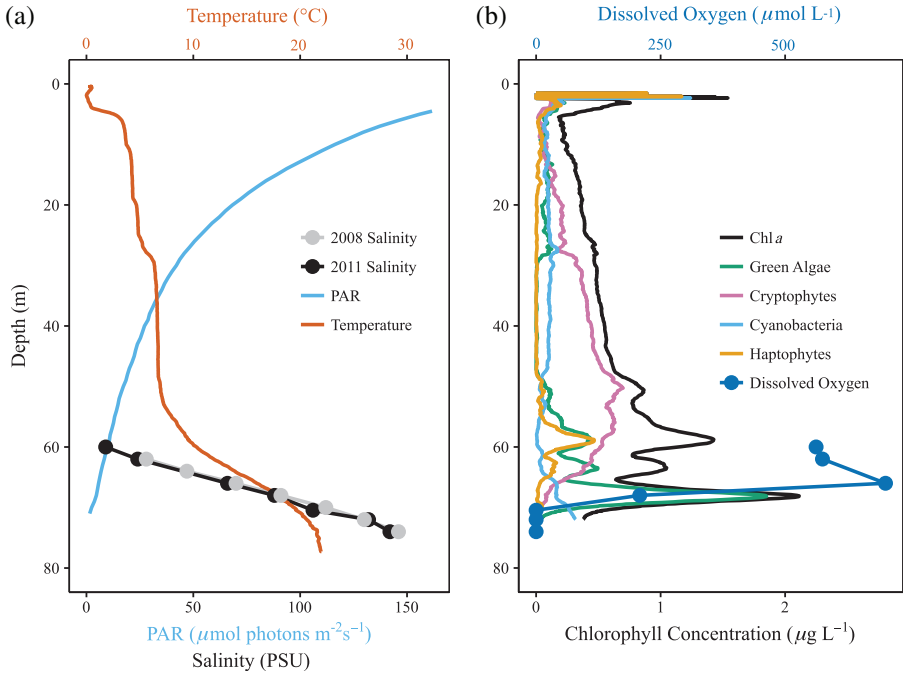

Fig. 1. (**a**) Photosynthetically active radiation and temperature profiles from 2011, and salinity profiles from 2008 and 2011. The 2008 salinity data are shifted downward by 2 m to correct for the increase in water level between the two field campaigns. (**b**) Chlorophyll (2 m running average) and dissolved oxygen concentration profiles from 2011.

regression, and b is the intercept. A further salinity correction was applied to the diffusion coefficient based on the concept that changes in diffusion coefficients are primarily driven by changes in the kinematic viscosity of water (Boudreau 1997) and can be calculated as:

$$\frac{D_B}{D_T} \approx \frac{\mu_T}{\mu_B} \tag{3}$$

where D_T and μ_T are the diffusion coefficient and kinematic viscosity of water, respectively, and D_B and μ_B are the diffusion coefficient and kinematic viscosity of brine, respectively. The kinematic viscosity of the calcium chloride brine along the salinity gradient in the deepest portions of Lake Vanda was calculated according to Phillips et al. (1981) equation for sodium chloride brines:

$$\frac{\mu_B}{\mu_T} = 1 + as + bs^2 + cs^3 + dT\left(1 - e^{ks}\right) \tag{4}$$

where $a = 0.0816$, $b = 0.0122$, $c = 0.000128$, $d = 0.000629$, $k = -0.7$, T is the temperature (°C), and s is the molar (mol kg^{-1}) concentration of salt, which was estimated from the measured salinity assuming that the brine was composed entirely of $CaCl_2$.

Depth-integrated net reaction rates were calculated as the area under the curve for positive and negative regions of the net reaction rate profiles using the auc function from the MESS package in R (Ekstrøm 2019).

Nitrification rate assay

Additional Lake Vanda water from 66 to 68 m was collected for use in potential rate assays. Lake water was filled into the bottom of a 1-liter polypropylene bottle and allowed to overflow. The bottle was sealed without headspace using a thick, butyl rubber stopper. This procedure minimized changes in dissolved gas concentrations due to sampling. This water was amended with 99 atom-% ^{15}N-ammonium to a final tracer concentration of 200 μmol L^{-1}. Taking into account the ambient ammonium concentrations measured in these samples (184–241 μmol L^{-1} at 66 m and 317–371 μmol L^{-1} at 68 m), the initial labeling of the ammonium pool in these incubations was 45–52 atom-% ^{15}N at 66 m and 35–39 atom-% ^{15}N at 68 m. Given the large in situ ammonium pools at these depths compared with very low half-saturation constants (< 1 μmol L^{-1}) typically observed for marine nitrifying microorganisms (Martens-Habbena et al. 2009), it is unlikely that this ammonium addition substantially altered the measured rates or affected the two depths differently. Samples (35 mL each) of labeled water from each depth were added to 27 base- and acid-washed and combusted 60-mL serum bottles. The vial headspace was ultra-high-purity air. Nine bottles from each depth received no further manipulation and were designated the "uninhibited" treatment. Five milliliters of methyl fluoride was added to each of nine additional vials to block the oxidation of ammonium to nitrite and inhibit nitrification (Miller et al. 1993), generating the "inhibited" treatment. The water in the final nine vials was filtered through two sterile,

0.2 μm syringe filters before being added to the vials. This was the "filtered control" treatment. Vials were incubated at 8°C. Three vials from each treatment at each depth were sacrificed at each of three time points after 0, 3, and 6 d of incubation. When each vial was sacrificed, the water it contained was filtered through 0.2 μm syringe filters and frozen. This frozen sample was used for analysis of ammonium, nitrate, and nitrite bulk concentrations as well as ^{15}N-nitrate. Last, the nitrate δ^{15}N values at each time point were used to calculate the rate of ^{15}N accumulation in the nitrate pool over time, allowing for estimation of nitrification rates using the atom fraction of ^{15}N in nitrate.

Determination of nitrate δ^{15}N and net nitrification rates

The "denitrifier method" was used to determine nitrate δ^{15}N ($\delta^{15}N_{NO_3}$) in water samples (Sigman et al. 2001; Casciotti et al. 2002). This method employs denitrifying bacteria that lack the N_2O reductase enzyme, which thereby convert NO_3^- to N_2O. The N_2O produced from this reaction is then measured by isotope ratio mass spectrometry. Prior to treating samples with denitrifying bacteria, sulfamic acid was added to water samples in order to remove NO_2^- (Granger and Sigman 2009). We performed this step because NO_2^- can also be utilized by denitrifying bacteria, and thus influence the isotopic signature of the N_2O measured. The nitrate isotope standards USGS32, USGS34, and USGS35 (Böhlke et al. 2003) were prepared and run in parallel with samples, and sample $\delta^{15}N_{NO_3}$ was determined relative to atmospheric N_2 and reported in units of per mil (‰).

Rates of nitrification were then calculated by accumulation of ^{15}N in the NO_3^- pool (Ward 2011). Knowing the ambient concentration and N isotopic composition of NO_3^- and NH_4^+ in Lake Vanda (Peters et al. 2014), the net nitrification rate was calculated as the change in the atom fraction ^{15}N in NO_3^- over the course of the incubation experiment (i.e., between 0 and 6 d).

Results

Physical and chemical structure of Lake Vanda

Water samples were collected from approximately the same location on Lake Vanda's surface in 2008 and 2011. The deepest depth that could be sampled with a Niskin bottle was 72 m in 2008 and 74 m in 2011. The concentration gradients measured in 2008 were shifted downward by 2 m to facilitate comparisons with the gradients measured in 2011. This shift provided the best match between the 2008 and 2011 salinity gradients (Fig. 1a). Assuming that the elevation of the salinity gradient above the lake bed remained constant, this observation qualitatively indicates a $\sim$ 2 m increase in the Lake Vanda water level over the 3-yr period between sample collections. Surface waters were characterized by low salinity and temperature. Below 60 m depth, salinity increased to a maximum value of around 150 PSU at the deepest depth sampled. The linear salinity gradient showed conservative diffusive mixing between fresh surface water and salty bottom water. Temperature also increased from a minimum of 0°C in the surface water to greater than 20°C in bottom waters (> 70 m). The pH decreased from 7.9 in surface waters to 6.0 in bottom waters.

Light penetration and pigment distribution

PAR was attenuated by 89% by the ice covering the surface of Lake Vanda, and by an additional 10% in the water between the bottom of the ice and the top of the salinity gradient (60 m, Fig. 1a). At 70 m depth, only 0.2% of incident PAR remained. Chl *a* concentrations in the Lake Vanda water column increased steadily with depth, reaching a series of deep, local maxima at 59.3, 63, and 68.2 m (Fig. 1b). The total chlorophyll signal was dominated by cryptophytes down to around 50 m depth after which green algae and haptophytes increased in abundance (Fig. 1b). The shallowest two chlorophyll maxima corresponded with peaks in the green algae and haptophyte signals, while the bottom maximum coincided with green algae only. While a cyanobacterial signal was present at low levels throughout the water column, it was a minor contributor to the deep chlorophyll maxima (Fig. 1b). The highest dissolved oxygen concentration was observed at 66 m, directly between the two deepest chlorophyll peaks (Fig. 1b).

Chemical gradients and diffusive fluxes

The chemical profiles measured in 2008 were shifted downward by 2 m such that the profiles measured in both 2008 and 2011 were in the same vertical position relative to the measured salinity gradients. Nitrous oxide had the shallowest local maximum at 62 m (Fig. 2). Dissolved oxygen, nitrate, and nitrite concentrations all had maxima at 66 m and decreased to zero by 70 m. Ammonium and DOC concentrations increased from nearly zero in surface waters to greater than 1 mmol L^{-1} near the lake bottom. Iron and manganese reached sharp concentration peaks at 70 m depth (Fig. 2 and Bratina et al. 1998). Methane and sulfide concentrations were undetectable throughout the upper water column and increased in the oxygen-depleted waters below 66 m for methane and 68 m for sulfide, both reaching maximum concentrations near the sediments (Fig. 2). High concentrations of the heavy metals vanadium, copper, cadmium, and barium were also observed within the salinity gradient, with lower concentrations in the freshwater above it (Supporting Information Table S1).

Net reaction rates and the vertical stratification of inferred biogeochemical processes

Net nitrous oxide and nitrate production was observed near the top of the salinity gradient down to a depth of $\sim$ 67 m, with maximum net nitrate production rates of 5–6 nmol L^{-1} d^{-1} (Fig. 3). Net nitrate production coincided with net ammonium consumption, consistent with nitrification activity, and a zone of net oxygen production. Net oxygen production from 63 to 67 m depth (Fig. 3) with a maximum activity of 26.6 nmol L^{-1} d^{-1} at

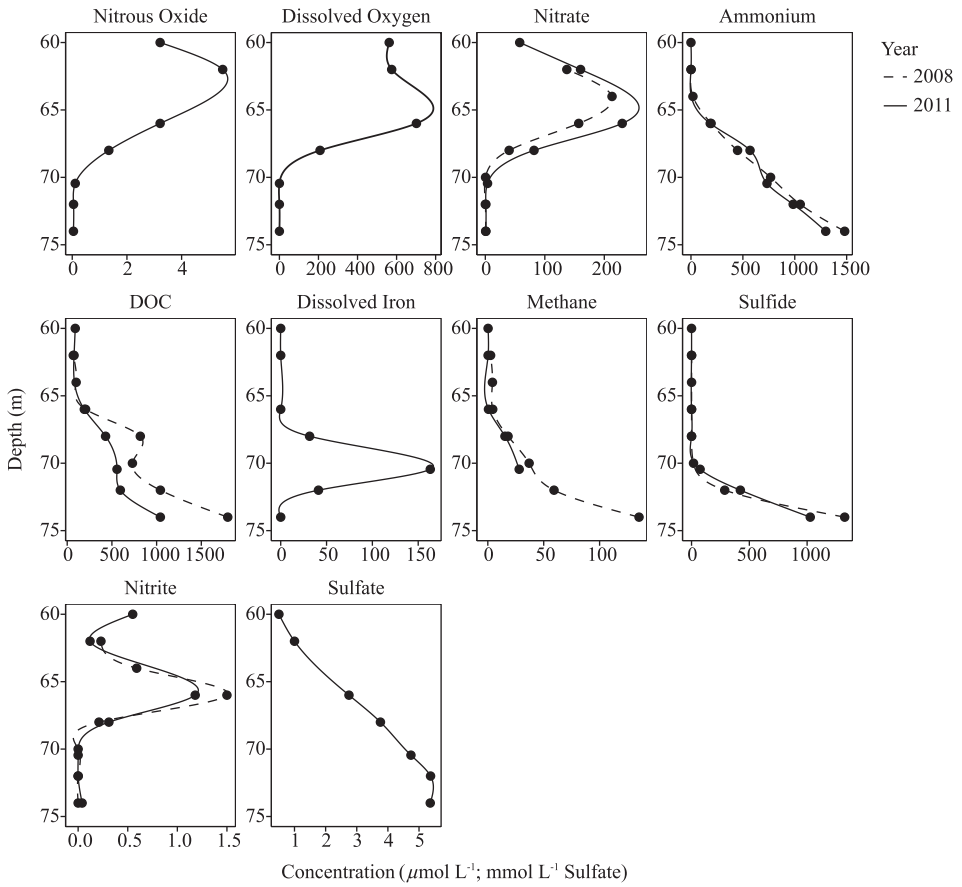

Fig. 2. Concentration depth profiles from 2008 and 2011. Nitrous oxide values are expressed on a per N atom basis. Sulfate concentrations are in mmol L^{-1}. Points represent measured values while the lines are natural cubic spline interpolations of those data. The panel labeled "Dissolved Iron" refers to total dissolved iron. Note that the 72 and 74 m methane data from 2011 are missing due to sample loss during analysis.

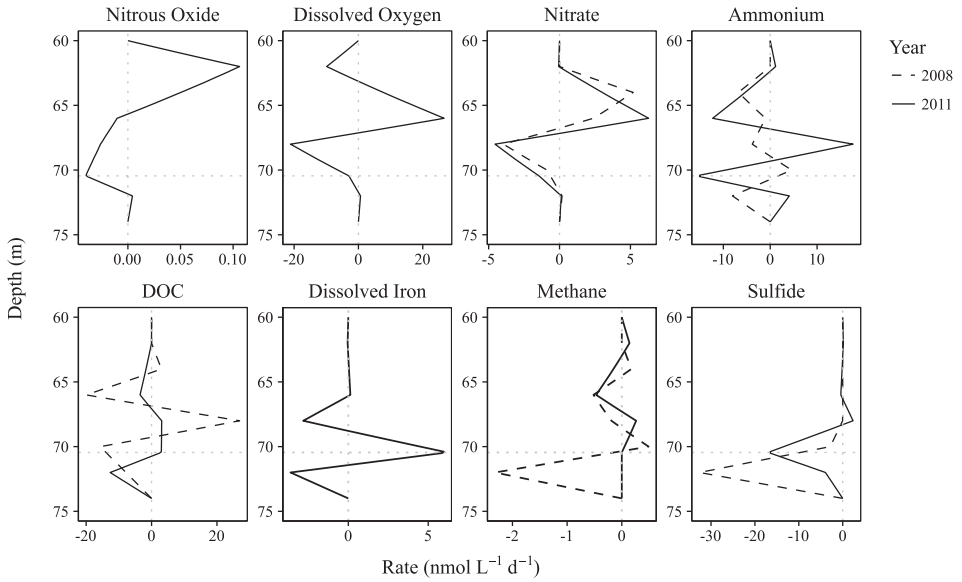

Fig. 3. Apparent net production (positive values) and consumption (negative values) rate profiles estimated using a reactive transport model (Eq. 1). The dotted vertical line shows where the net reaction rate is zero and the dotted horizontal line shows the depth at which dissolved oxygen concentrations reached zero. The panel labeled "Dissolved Iron" refers to total dissolved iron.

66 m depth was driven by oxygenic photosynthesis (Table 1). Net methane consumption from 63 to 68 m (Fig. 3) was attributed to aerobic methane oxidation (Table 1). A net loss of total dissolved iron from 66 to 69 m depth (Fig. 3) in the presence of oxygen (Fig. 2) was most likely driven by Fe(II) oxidation and the formation of particulate iron oxide minerals (Table 1). Net nitrate consumption combined with net nitrous oxide consumption over the 67–72 m depth interval (Fig. 3) suggests a zone of water column denitrification (Table 1). Net sulfide loss was also observed within this depth range (Fig. 3), indicating sulfide oxidation activity (Table 1).

Oxygen and nitrate were not detectable below a depth of ~ 70 m (Fig. 2), and thus a different suite of biogeochemical processes became active in deeper waters (Table 1). Net production of total dissolved iron at the oxycline (Fig. 3) likely resulted from the reduction of particulate iron and its subsequent dissolution (Table 1). Net consumption of dissolved iron and sulfide in deep waters (Fig. 3) was likely driven by iron-sulfide precipitation (Table 1), perhaps combined with anoxygenic photosynthesis in the case of sulfide. Net deep-water methane consumption (Fig. 3) resulted from the anaerobic oxidation of methane (Table 1).

Table 1. Vertical stratification of inferred biogeochemical processes along with net metabolite production (+) and consumption (–) rates expressed as depth-integrated net areal rates.

Inferred biogeochemical process (approximate depth range)	Metabolite	Year	Integrated net rate (μmol m^{-2} d^{-1})
Nitrification (60–67 m)	N_2O	2011	+0.3
	NO_3^-	2008	+13.7
		2011	+15.9
Aerobic respiration (60–70 m)	O_2	2011	–15.4
		2011	–40.9
Oxygenic photosynthesis (63–67 m)	O_2	2011	+52.3
Aerobic methane oxidation (63–68 m)	CH_4	2008	–1.1
		2011	–1.0
Iron oxide particle formation (66–69 m)	Fe	2011	–3.8
Denitrification (66–72 m)	NO_3^-	2008	–8.1
		2011	–10.3
	N_2O	2011	–0.1
Iron particle dissolution (69–72 m)	Fe	2011	+8.1
Total sulfide consumption	HS^-	2008	–71.0
		2011	–38.3
Iron-sulfide precipitation (70–74 m)	Fe	2011	–4.7
Sulfide oxidation (total consumption – precipitation) (66–70 m)	HS^-	2008	–66.3
		2011	–33.6
Anaerobic methane oxidation (70–74 m)	CH_4	2008	–4.2

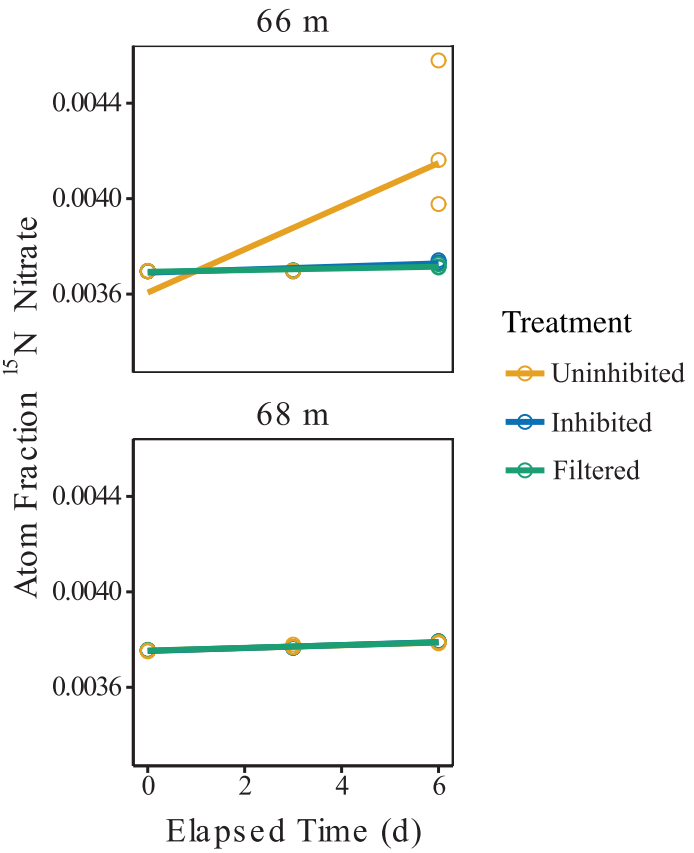

Fig. 4. ^{15}N accumulation through time in the nitrate pool following enrichment with $^{15}NH_4^+$ in samples from 66 and 68 m depth. Nitrification inhibition was achieved through the addition of methyl fluoride. [Color figure can be viewed at wileyonlinelibrary.com]

^{15}N incubations

Nitrification activity was confirmed at 66 m by accumulation of ^{15}N-NO_3 following incubation with ^{15}N-NH_4 (Fig. 4). The average nitrification rate measured in the uninhibited treatment at this depth was 40 ± 13 nmol L^{-1} d^{-1} (Table 2), an order of magnitude higher than the 5–6 nmol L^{-1} d^{-1} rate

Table 2. Nitrification rates measured in the Lake Vanda water column.

Depth (m)	Treatment	Nitrification rate (nmol L^{-1} d^{-1})
66	Inhibited	2.8 ± 0.6
	Killed	1.5 ± 0.3
	Uninhibited	40 ± 13
68	Inhibited	1.0 ± 0.1
	Killed	0.9 ± 0.1
	Uninhibited	0.9 ± 0.1

of net nitrate production at this depth estimated from the nitrate concentration profile (Fig. 3). The ^{15}N incubation experiment confirmed that there was no detectable nitrification activity in water collected from 68 m depth (Table 2).

Discussion

Temporal stability of Lake Vanda geochemical gradients

We collected water column samples from the same GPS coordinates on Lake Vanda in 2008 and 2011. In 2011, we collected a sample from 2 m deeper than the deepest sample we could collect in 2008. This rough measurement of the change in depth of the lake agrees well with the analyses of Castendyk et al. (2016), who used detailed lake bathymetry combined with a time series of aerial and satellite images of the lake surface to calculate the depth of Lake Vanda. In spite of the change in lake depth, the shape of the geochemical gradients and their relative position in the water column remained constant. These gradients also agree well with previous reports (Canfield and Green 1993; Voytek et al. 1999; Green and Lyons 2009). Green and Lyons (2009) commented on the remarkable stability of chemical gradients in the Lake Vanda brine since at least the 1980s despite the significant changes in lake level that have occurred. By keeping the sampling location constant between sampling events, our measurements confirm that this chemical stability persists.

Photosynthesis and pigment distribution

Light penetrates nearly to the bottom of Lake Vanda, allowing deep photosynthesis to take place where more nutrients are available and the water is warmer (Vincent and Vincent 1982; Vincent et al. 1998). Indeed, the Lake Vanda deep chlorophyll maxima at 59.3, 63, and 68.2 m (Fig. 1) span the top of the salinity gradient where concentrations of dissolved inorganic nutrients like phosphate (Canfield and Green 1993) and nitrate and ammonium (Fig. 2) are present far in excess of concentrations observed in fresh surface waters (Fig. 2). The vertical position of the deep chlorophyll maximum can be explained by a combination of factors, including nutrient and light availability, cell buoyancy over a steep density gradient, and inhibition of biological activity by high heavy metal concentrations in deeper waters (Burnett et al. 2006). Interestingly, net oxygen production was only observed in the 63–67 m depth range, with peak activity at 66 m, directly between two of the deep chlorophyll maxima. The deepest two of the chlorophyll maxima were in fact zones of net oxygen consumption (Fig. 3; Table 1). In addition to Chl *a*, none of the four major spectral phytoplankton groups (green algae, cryptophytes, cyanobacteria, and haptophytes) distinguishable by our method had a local maximum corresponding with the dissolved oxygen peak (Fig. 1b). Therefore, the net oxygen production observed there cannot be explained by a small but very active phytoplankton subgroup corresponding with one of our measured spectral groups.

There are several possible explanations for the vertical offset between net oxygen production and chlorophyll maxima. First, it must be noted that the deeper chlorophyll maxima may reflect a physiological response of some phytoplankton to low light conditions and therefore may not necessarily suggest a zone of enhanced photosynthetic activity or phytoplankton abundance (Falkowski 1980). Furthermore, mixotrophy may be an important strategy for phytoplankton growth in these extremely eutrophic waters (Li et al. 2019), such that increased phytoplankton abundance may not result in net oxygen production. Another possibility is that active phytoplankton cells were more buoyant than inactive cells, as has been previously described for marine phytoplankton (Steele and Yentsch 1960). A small number of photosynthetically active cells may have floated higher than their more numerous inactive (or possibly dead) counterparts in the steep density gradient that exists at this depth in the water column, creating the observed peak in net oxygen production above the largest of the peaks in chlorophyll concentration. Finally, it is possible that a large amount of oxygen was generated at the observed oxygen concentration maximum early in the Antarctic spring when light first became available, after which primary production activity shifted to different depths in the water column following seasonally fluctuating light (Fritsen and Priscu 1999) and nutrient gradients (Kong et al. 2012). That is, nutrient gradients were measured at the same time of year in 2008 and 2011 such that they were very stable year-to-year, but this sampling regime may have missed seasonal fluctuations in nutrient gradients caused by light- and temperature-driven changes in biological processes.

Nitrification and nitrous oxide production

Nitrification activity, inferred from observed nitrate production (Fig. 3) and confirmed through stable isotope incubations (Fig. 4; Table 2), was observed near the top of the salinity gradient (Table 1), as reported previously (Vincent and Downes 1981; Canfield and Green 1993; Voytek et al. 1999). The rate of net nitrous oxide production observed at the same depth was only a small fraction ($\sim$ 2%) of the net nitrate production rate (Table 1), suggesting that nitrification was sufficient to explain the net production of both nitrous oxide and nitrate. Since net nitrous oxide production occurred at a shallower depth than net oxygen production (Fig. 3; Table 1), it is unlikely that nitrous oxide was a byproduct of phytoplankton assimilatory nitrate reduction (Vincent and Downes 1981). Abiotic nitrous oxide production was also unlikely because this production pathway requires ferrous iron to reduce nitrite to nitrous oxide (Samarkin et al. 2010). No dissolved iron was observed at the depths where nitrous oxide production was observed, and any particulate iron would likely be in the ferric form, since oxygen was also present in this zone. These data support the contention that nitrous oxide was produced by classical nitrification (Voytek et al. 1999; Peters et al. 2014).

Surprisingly, no net nitrate production was observed at 68 m where oxygen and ammonium gradients overlapped

(Fig. 3; Table 1). The lack of nitrification at this depth was corroborated by ^{15}N incubations, which also showed no detectable activity (Fig. 4; Table 2). Given that sufficient substrates were available for nitrification, it is likely that the process was inhibited. H_2S, a known nitrification inhibitor (Joye and Hollibaugh 1995), was not present, as total sulfide concentrations were not detectable above 70 m depth (Fig. 2). Light or oxygen radicals are other possible inhibitors of nitrification (Tolar et al. 2016), but these are unlikely as well, as nitrification was active in shallower water where more light was present. Methane, however, was present at 68 m (Fig. 2) and it could inhibit nitrification at this depth. Ammonia monooxygenase and methane monooxygenase are similar enzymes, and methane and ammonia are substrates for both enzymes. Methane thus competes with ammonia for the activity of ammonia monooxygenase; in this regard, methane was shown to inhibit nitrification in pure cultures of nitrifying microorganisms (Bédard and Knowles 1989) and in soil microcosms (Zheng et al. 2014). Though ammonium concentrations at 68 m were greater than 500 μmol L^{-1}, the actual substrate for the ammonia monooxygenase enzyme that catalyzes the first step in the nitrification reaction is ammonia. The ammonia concentration at 68 m was calculated to be μmol L^{-1} based on the acid-base equilibrium of ammonia and ammonium, assuming a pH of 6.3 and pK_a of 9.3 (Beman et al. 2011). The methane concentration at 68 m was 15 μmol L^{-1}, over 20 times higher than the calculated ammonia concentration. Thus, we hypothesize that competitive inhibition of ammonia monooxygenase by methane may have caused the observed lack of ammonia oxidation activity in 68 m samples (Bédard and Knowles 1989; Zheng et al. 2014). The observation of net methane consumption at this depth from the more complete 2008 depth profile is consistent with this hypothesis (Fig. 3).

Reductive nitrogen-cycling processes

Most of the observed net nitrate and nitrous oxide consumption took place above the oxycline (70 m, the depth at which oxygen disappeared). Given that denitrifying microorganisms are facultative anaerobes, the most probable pathway for nitrate consumption was assimilation. However, nitrous oxide was also consumed at this depth, suggesting denitrification activity. It is possible that denitrification was active in the anoxic core of sinking particles. While Lake Vanda surface waters are exceptionally oligotrophic with low cell densities and high light transmittance, suggesting a low particle concentration, net DOC and ammonium production within the $\sim$ 66–70 m depth range (Fig. 3) was consistent with microbial mineralization of particulate organic matter produced in the shallower zone of photosynthesis. These organic particles may have provided an anoxic microenvironment that could support anaerobic denitrification. It is also possible that aerobic denitrification drove some of the observed nitrate and nitrous oxide consumption above the oxycline. This process has been observed in laboratory incubations (Lloyd et al. 1987) and in intertidal sediments (Gao et al. 2010), but has never been described in an extreme environment, making it an interesting topic for future research.

Metal and sulfur chemistry

The peak in dissolved iron at the oxycline supports the model for metal cycling in Lake Vanda proposed by Green and Lyons (2009). They proposed that metals are delivered to the lake via the Onyx River and that they form metal oxide particles in the oxic surface layer. These particles sink to the oxycline where they are reduced and dissolved in the absence of oxygen, creating the characteristic dissolved iron peak observed in our study in both 2008 and 2011. Reduced metals diffusing upward from 70 m are reoxidized and sink again, while those diffusing downward precipitate with sulfide and are buried in the sediment. Indeed, much of the upward diffusing sulfide flux was apparently consumed in the anoxic bottom waters of Lake Vanda (Table 1), probably by metal precipitation, with possible additional contributions by phototrophic sulfur bacteria (Kriss et al. 1976; Takii et al. 1986), though only 0.2% (2.4 μmol photons m^{-2} s^{-1}) of incident PAR penetrated to 70 m depth (Fig. 1). The sulfide that escaped metal precipitation was oxidized completely just above the oxycline, presumably by sulfur-oxidizing chemolithotrophs that consumed some of the downward flux of oxygen or nitrate as electron acceptors. Corroborating this idea, Dolhi et al. (2015) reported the presence of genes encoding ribulose bisphosphate carboxylase related to sulfur-oxidizing bacteria in the deep waters of Lake Vanda. Therefore, the sulfide flux from the sediment or near bottom water to the water column represents an energy flux that is likely important to maintaining the energy balance of the deep-water microbial community. This sulfide flux is likely driven by sulfate reduction at or near the sediment surface, which is consistent with the sulfate concentration at 74 m being lower than one would expect based on the otherwise linear sulfate profile. It is worth noting that the large differences in sulfide consumption and oxidation rates between 2008 and 2011 were likely the result of the steep sulfide concentration gradient combined with the coarse (2 m) sampling resolution. The substantially higher bottom water (74 m) sulfide concentration measured in 2008 compared with 2011 probably resulted from the Niskin sampler being slightly closer to the lake bottom.

Methane cycling

In most marine environments where sulfate is available as an electron acceptor, anaerobic oxidation of methane is coupled with sulfate reduction (Boetius et al. 2000). Indeed, sulfate concentrations were high (0.5–5.3 mmol L^{-1}) in Lake Vanda bottom waters (Fig. 2) where net methane consumption was observed under anoxic conditions (70–74 m; Fig. 3). Other electron acceptors, such as nitrite, can also drive anaerobic methanotrophy (Ettwig et al. 2008). Nitrite was shown to be the dominant electron acceptor for anaerobic methane oxidation in Lake

Constance sediments (Deutzmann et al. 2014), and genomic evidence for this process was found in the water columns of two Tibetan saline lakes as well (Yang et al. 2012). However, no nitrite was found below 70 m depth in Lake Vanda (Fig. 2). Thus sulfate, or some electron acceptor not identified in our work, must support the anaerobic methane oxidation observed in the Lake Vanda brine.

In spite of anaerobic methane oxidation, some methane penetrated into oxic Lake Vanda waters (Fig. 2), allowing for aerobic methane oxidation from 63 to 68 m depth (Fig. 3; Table 1). This pattern is similar to that observed in other saline lakes such as Mono Lake (Joye et al. 1999) and Big Soda Lake (Iversen et al. 1987). However, in contrast with Mono Lake, where maximum aerobic methanotrophy rates were concentrated in barely oxic waters directly above the oxycline (Carini et al. 2005), aerobic methanotrophy in Lake Vanda was concentrated farther above the oxycline where oxygen concentrations were much higher. While both aerobic and anaerobic methane oxidation were inferred to be active in Lake Vanda (Fig. 3), the majority of the methane diffusing upward from the lake bottom was consumed in the anoxic portion of the water column below 70 m (Table 1).

Balance of electron acceptors and electron donors at the oxycline

The confluence of downward diffusing terminal electron acceptors (oxygen and nitrate) with upward diffusing electron donors (sulfide) at the oxycline ($\sim$ 70 m, Fig. 2) provides the opportunity to test the quality of these concentration profile-based rate calculations. In theory, these fluxes should balance one another under the assumption that the other upward diffusing electron donors (ammonium, methane, and DOC) are primarily oxidized higher in the water column as indicated by their concentration profiles (Fig. 2). The integrated net sulfide oxidation rate near the oxycline, after accounting for sulfide loss through iron coprecipitation, ranged from 33.6 to 66.3 μmol m^{-2} d^{-1} between the 2 yr sampled (Table 1). The integrated net oxygen consumption rate at this depth was 40.9 μmol m^{-2} d^{-1} (Table 1), sufficient to oxidize 20.5 μmol m^{-2} d^{-1} of sulfide assuming a 2:1 oxygen:sulfide reaction stoichiometry (Canfield et al. 1993).

Integrated net nitrate reduction rates ranged from 8.1 to 10.3 μmol m^{-2} d^{-1} between 2008 and 2011 (Table 1). Assuming a 1.6:1 nitrate:sulfide reaction stoichiometry for autotrophic denitrification (Schutte et al. 2018), this was sufficient to oxidize 5.1–6.4 μmol m^{-2} d^{-1} of sulfide. Total sulfide oxidation by the combination of these two terminal electron acceptors was 25.6–26.9 μmol m^{-2} d^{-1}, somewhat less than the calculated sulfide oxidation rate. It is possible that some of this discrepancy could be caused by sulfide oxidation via anoxygenic photosynthesis, a process coupled to CO_2 fixation and independent of exogenous electron acceptors such as nitrate or oxygen. It is also possible that this difference is due to uncertainties in the underlying concentration data. The most important of which is likely the low spatial resolution (2 m) at which samples were collected. With this broad of a sampling interval, it is possible that the actual oxygen and nitrate peaks were not sampled, ultimately deflating their calculated diffusive fluxes and reaction rates.

Temporal stability of the vertical stratification of biogeochemical processes in the Lake Vanda water column

The vertical stratification of biogeochemical processes in Lake Vanda appears to be consistent through time, extending as far back as Canfield et al. (1985) who first showed a layer of nitrification overlying a layer of photosynthesis overlying a layer of denitrification. However, it was not only the relative position in the water column of the biogeochemical processes that remained constant between 2008 and 2011; the net volumetric reaction rates (Fig. 3) and integrated areal rates (Table 1) of many of the nitrogen- and metal-cycling processes were remarkably consistent between the two sampling dates as well. Our integrated approach to the study of Lake Vanda water column chemistry agrees with this study and revealed several other key insights into the biogeochemical functioning of the lake:

1. The depth of maximum net oxygen production did not coincide with any of three deep chlorophyll maxima (at 59.3, 63, and 68.2 m). This pattern could be driven by a decoupling between chlorophyll concentration and net photosynthetic activity at the organismal level or by seasonal fluctuations in phytoplankton location or activity that are not captured in our "snapshots" of the Lake Vanda water column.
2. No nitrification activity was observed at 68 m depth in spite of overlapping oxygen and ammonium gradients. We attribute this lack of activity to the competitive inhibition of ammonia monooxygenase by methane.
3. Net nitrous oxide and nitrate consumption were observed in the oxic water column, suggesting the possibility that aerobic denitrification may be active in this extreme (high salinity) environment.

References

Bédard, C., and R. Knowles. 1989. Physiology, biochemistry, and specific inhibitors of CH_4, NH_4^+, and CO oxidation by methanotrophs and nitrifiers. Microbiol. Rev. **53**: 68–84.

Beman, J. M., and others. 2011. Global declines in oceanic nitrification rates as a consequence of ocean acidification. Proc. Natl. Acad. Sci. USA **108**: 208–213. doi:10.1073/pnas.1011053108

Bendschneider, K., and R. J. Robinson. 1952. A new spectrophotometric method for the determination of nitrite in sea water. J. Mar. Res. **11**: 87–96.

Berner, R. A. 1980. Early diagenesis: A theoretical approach. Princeton Univ. Press.

Beutler, M., and others. 2002. A fluorometric method for the differentiation of algal populations in vivo and in situ. Photosynth. Res. **72**: 39–53. doi:10.1023/A:1016026607048

Bielewicz, S., E. Bell, W. Kong, I. Friedberg, J. C. Priscu, and R. M. Morgan-Kiss. 2011. Protist diversity in a permanently ice-covered Antarctic lake during the polar night transition. ISME J. **5**: 1559–1564. doi:10.1038/ismej.2011.23

Boetius, A., and others. 2000. A marine microbial consortium apparently mediating anaerobic oxidation of methane. Nature **407**: 623–626. doi:10.1038/35036572

Böhlke, J. K., S. J. Mroczkowski, and T. B. Coplen. 2003. Oxygen isotopes in nitrate: New reference materials for ^{18}O:^{17}O:^{16}O measurements and observations on nitrate-water equilibration. Rapid Commun. Mass Spectrom. **17**: 1835–1846. doi:10.1002/rcm.1123

Boudreau, B. P. 1997. Diagenetic models and their implementation. Springer.

Bratina, B. J., B. S. Stevenson, W. J. Green, and T. M. Schmidt. 1998. Mangenese reduction by microbes from oxic regions of the Lake Vanda (Antarctica) water column. Appl. Environ. Microbiol. **64**: 3791–3797.

Burnett, L., D. Moorhead, I. Hawes, and C. Howard-Williams. 2006. Environmental factors associated with deep chlorophyll maxima in dry valleys lakes, South Victoria land, Antarctica. Arct. Antarct. Alp. Res. **38**: 179–189. doi:10.1657/1523-0430(2006)38[179:EFAWDC]2.0.CO;2

Canfield, D. E., and W. J. Green. 1985. The cycling of nutrients in a closed-basin antarctic lake: Lake Vanda. Biogeochemistry **1**: 233–256. doi:10.1007/BF02187201

Canfield, D. E., B. Thramdrup, and J. W. Hansen. 1993. The anaerobic degradation of organic carbon in Danish coastal sediments: Iron reduction, manganese reduction and sulfate reduction. Geochim. Cosmochim. Acta **57L**: 3867–3883.

Canfield, D. E., and others. 1993. Pathways of organic carbon oxidation in three continental margin sediments. Mar. Geol. **113**: 27–40. doi:10.1016/0025-3227(93)90147-N

Carini, S., N. Bano, G. LeCleir, and S. B. Joye. 2005. Aerobic methane oxidation and methanotroph community composition during seasonal stratification in Mono Lake, California (USA). Environ. Microbiol. **7**: 1127–1138. doi:10.1111/j.1462-2920.2005.00786.x

Casciotti, K. L., D. M. Sigman, M. G. Hastings, J. K. Böhlke, and A. Hilkert. 2002. Measurement of the oxygen isotopic composition of nitrate in seawater and freshwater using the denitrifier method. Anal. Chem. **74**: 4905–4912. doi:10.1021/ac020113w

Castendyk, D. N., M. K. Obryk, S. Z. Leidman, M. Gooseff, and I. Hawes. 2016. Lake Vanda: A sentinel for climate change in the McMurdo Sound Region of Antarctica. Glob. Planet. Change **144**: 213–227. doi:10.1016/j.gloplacha.2016.06.007

Cline, J. D. 1969. Spectrophotometric determination of hydrogen sulfide in natural waters. Limnol. Oceanogr. **14**: 454–458. doi:10.4319/lo.1969.14.3.0454

Deutzmann, J. S., P. Stief, J. Brandes, and B. Schink. 2014. Anaerobic methane oxidation coupled to denitrification is the dominant methane sink in a deep lake. Proc. Natl. Acad. Sci. USA **111**: 18273–18278. doi:10.1073/pnas.1411617111

Dolhi, J. M., A. G. Teufel, W. Kong, and R. M. Morgan-Kiss. 2015. Diversity and spatial distribution of autotrophic communities within and between ice-covered Antarctic lakes (McMurdo Dry Valleys). Limnol. Oceanogr. **60**: 977–991. doi:10.1002/lno.10071

Ekstrøm, C. T. 2019. MESS: Mescellaneous esoteric statistical scripts. R package version 0.5.5. https://CRAN.R-project.org/package=MES

Ettwig, K. F., and others. 2008. Denitrifying bacteria anaerobically oxidize methane in the absence of Archaea. Environ. Microbiol. **10**: 3164–3173. doi:10.1111/j.1462-2920.2008.01724.x

Falkowski, P. G. 1980. Light-shade adaptation in marine phytoplankton, p. 99–119. *In* P. G. Falkowski [ed.], Primary productivity in the sea. Environmental science research. Springer.

Fritsen, C. H., and J. C. Priscu. 1999. Seasonal change in the optical properties of the permanent ice cover on Lake Bonney, Antarctica: Consequences for lake productivity and phytoplankton dynamics. Limnol. Oceanogr. **44**: 447–454. doi:10.4319/lo.1999.44.2.0447

Gao, H., and others. 2010. Aerobic denitrification in permeable Wadden Sea sediments. ISME J. **4**: 417–426. doi:10.1038/ismej.2009.127

Granger, J., and D. M. Sigman. 2009. Removal of nitrite with sulfamic acid for nitrate N and O isotope analysis with the denitrifier method. Rapid Commun. Mass Spectrom. **23**: 3753–3762. doi:10.1002/rcm.4307

Green, W. J., and W. B. Lyons. 2009. The saline lakes of the McMurdo Dry Valleys, Antarctica. Aquat. Geochem. **15**: 321–348. doi:10.1007/s10498-008-9052-1

Hoare, R. A. 1966. Problems of heat transfer in Lake Vanda, a density stratified Antarctic lake. Nature **210**: 787–789. doi:10.1038/210787a0

Iversen, N., R. S. Oremland, and M. J. Klug. 1987. Big Soda Lake (Nevada). 3. Pelagic methanogenesis and anaerobic methane oxidation. Limnol. Oceanogr. **32**: 804–814. doi:10.4319/lo.1987.32.4.0804

Joye, S. B., and J. T. Hollibaugh. 1995. Influence of sulfide inhibition of nitrification on nitrogen regeneration in sediments. Science **270**: 623–625. doi:10.1126/science.270.5236.623

Joye, S. B., T. L. Connell, L. G. Miller, R. S. Oremland, and R. S. Jellison. 1999. Oxidation of ammonia and methane in an alkaline, saline lake. Limnol. Oceanogr. **44**: 178–188. doi:10.4319/lo.1999.44.1.0178

Kong, W., D. C. Ream, J. C. Priscu, and R. M. Morgan-Kiss. 2012. Diversity and expression of RubisCO genes in a perennially ice-covered Antarctic lake during the polar night transition. Appl. Environ. Microbiol. **78**: 4358–4366. doi:10.1128/AEM.00029-12

Kriss, A. E., I. N. Mitskevich, E. P. Rozanova, and L. K. O'Snitskaya. 1976. Microbiological investigations of Lake Vanda (Antarctica). Microbiology **45**: 917–922.

Li, W., J. Dolhi-Binder, Z. Cariani, and R. Morgan-Kiss. 2019. Drivers of protistan community autotrophy and heterotrophy in chemically stratified Antarctic lakes. Aquat. Microb. Ecol. **82**: 225–239. doi:10.3354/ame01891

Lloyd, D., L. Boddy, and K. J. P. Davies. 1987. Persistence of bacterial denitrification capacity under aerobic conditions: The rule rather than the exception. FEMS Microbiol. Ecol. **45**: 185–190. doi:10.1111/j.1574-6968.1987.tb02354.x

Martens-Habbena, W., P. M. Berube, H. Urakawa, J. R. de la Torre, and D. A. Stahl. 2009. Ammonia oxidation kinetics determine niche separation of nitrifying Archaea and Bacteria. Nature **461**: 976–981. doi:10.1038/nature08465

Miller, L. G., M. D. Coutlakis, R. S. Oremland, and B. B. Ward. 1993. Selective inhibition of ammonium oxidation and nitrification-linked N_2O formation by methyl fluoride and dimethyl ether. Appl. Environ. Microbiol. **59**: 2457–2464.

Peters, B., K. L. Casciotti, V. A. Samarkin, M. T. Madigan, C. A. Schutte, and S. B. Joye. 2014. Stable isotope analyses of NO_2^-, NO_3^-, and N_2O in the hypersaline ponds and soils of the McMurdo Dry Valleys, Antarctica. Geochim. Cosmochim. Acta **135**: 87–101. doi:10.1016/j.gca.2014.03.024

Phillips, S. L., A. Igbene, J. A. Fair, H. Ozbek, and M. Tavana. 1981. A technical databook for geothermal energy utilization. Lawrence Berkeley Laboratory.

R Core Team. 2017. R: A language and environment for statistical computing. R Foundation for Statistical Computing.

Ragotzkie, R. A., and G. E. Likens. 1964. The heat balance of two Antarctic lakes. Limnol. Oceanogr **9**: 412–425.

Samarkin, V. A., and others. 2010. Abiotic nitrous oxide emission from the hypersaline Don Juan Pond in Antarctica. Nat. Geosci. **3**: 341–344. doi:10.1038/ngeo847

Saxton, M. A., and others. 2016. Biogeochemical and 16S rRNA gene sequence evidence supports a novel mode of anaerobic methanotrophy in permanently ice-covered Lake Fryxell, Antarctica. Limnol. Oceanogr. **61**: S119–S130. doi:10.1002/lno.10320

Schmid, M., A. Lorke, C. Dinkel, G. Tanyileke, and A. Wüest. 2004. Double-diffusive convection in Lake Nyos, Cameroon. Deep-Sea Res. Part I Oceanogr. Res. Pap. **51**: 1097–1111. doi:10.1016/j.dsr.2004.02.010

Schmid, M., M. Busbridge, and A. Wüest. 2010. Double-diffusive convection in Lake Kivu. Limnol. Oceanogr. **55**: 225–238. doi:10.4319/lo.2010.55.1.0225

Schulz, H. D., and M. Zabel. 2006. Marine geochemistry. Springer.

Schutte, C. A., and others. 2018. Filamentous giant *Beggiatoaceae* from the Guaymas Basin are capable of both denitrification and dissimilatory nitrate reduction to ammonium. Appl. Environ. Microbiol. **84**: e02860–17. doi:10.1128/AEM.02860-17

Sigman, D. M., K. L. Casciotti, M. Andreani, C. Barford, M. Galanter, and J. K. Böhlke. 2001. A bacterial method for the nitrogen isotopic analysis of nitrate in seawater and freshwater. Anal. Chem. **73**: 4145–4153. doi:10.1021/ac010088e

Solorzano, L. 1969. Determination of ammonia in natural waters by the phenolhypochlorite method. Limnol. Oceanogr. **14**: 799–801. doi:10.4319/lo.1969.14.5.0799

Steele, J. H., and C. S. Yentsch. 1960. The vertical distribution of chlorophyll. J. Mar. Biol. Assoc. U.K. **39**: 217–226. doi:10.1017/S0025315400013266

Takii, S., T. Konda, A. Hiraishi, G. I. Matsumoto, T. Kawano, and T. Torii. 1986. Vertical distribution in and isolation of bacteria from Lake Vanda: An Antarctic lake. Hydrobiologia **135**: 15–21. doi:10.1007/BF00006454

Tolar, B. B., L. C. Powers, W. L. Miller, N. J. Wallsgrove, B. N. Popp, and J. T. Hollibaugh. 2016. Ammonia oxidation in the ocean can be inhibited by nanomolar concentrations of hydrogen peroxide. Front. Mar. Sci. **3**: 237. doi:10.3389/fmars.2016.00237

Tregoning, G. S., M. L. Kempher, D. O. Jung, V. A. Samarkin, S. B. Joye, and M. T. Madigan. 2015. A halophilic bacterium inhabiting the warm, $CaCl_2$-rich brine of the perennially ice-covered Lake Vanda, McMurdo Dry Valleys, Antarctica. Appl. Environ. Microbiol. **81**: 1988–1995. doi:10.1128/AEM.03968-14

Vincent, W. F., and M. T. Downes. 1981. Nitrous oxide cycling in Lake Vanda, Antarctica. Nature **292**: 618–620. doi:10.1038/292618a0

Vincent, W. F., and C. L. Vincent. 1982. Factors controlling phytoplankton production in Lake Vanda (77°S). Can. J. Fish. Aquat. Sci. **39**: 1602–1609. doi:10.1139/f82-216

Vincent, W. F., R. Rae, I. Laurion, C. Howard-Williams, and J. C. Priscu. 1998. Transparency of Antarctic ice-covered lakes to solar UV radiation. Limnol. Oceanogr. **43**: 618–624. doi:10.4319/lo.1998.43.4.0618

Voytek, M. A., J. C. Priscu, and B. B. Ward. 1999. The distribution and relative abundance of ammonia-oxidizing bacteria in lakes of the McMurdo Dry Valley, Antarctica. Hydrobiologia **401**: 113–130. doi:10.1023/A:1003754830988

Ward, B. B. 2011. Measurement and distribution of nitrification rates in the oceans, p. 307–323. *In* M. G. Klotz [ed.], Methods in enzymology. Academic Press.

Wilson, A. T. 1964. Evidence from chemical diffusion of a climatic change in the McMurdo Dry Valleys 1,200 years ago. Nature **201**: 176–177. doi:10.1038/201176b0

Yang, J., and others. 2012. Co-occurrence of nitrite-dependent anaerobic methane oxidizing and anaerobic ammonia oxidizing bacteria in two Qinghai-Tibetan saline lakes. Front. Earth Sci. **6**: 383–391. doi:10.1007/s11707-012-0336-9

Zheng, Y., R. Huang, B. Z. Wang, P. L. E. Bodelier, and Z. J. Jia. 2014. Competitive interactions between methane- and ammonia-oxidizing bacteria modulate carbon and nitrogen

cycling in paddy soil. Biogeosciences **11**: 3353–3368. doi: 10.5194/bg-11-3353-2014

Acknowledgments

We thank Jenna Dolhi-Binder and Nick Ketchum for their help with field work in 2011 and all of the staff at McMurdo Station including Petroleum Helicopters, Inc. for making our research possible. Kim Hunter provided invaluable support with sample analysis. Dirk de Beer gave feedback on an early version of this manuscript that helped improve it immensely. This work was funded by a grant from the National Science Foundation (award ANT-0735196 to SJ, MTM, and VAS) and the National Aeronautics and Space Administration (Exobiology/Astrobiology award NNX11AG45G to SJ, MTM, VAS, and KC). RMK was supported by the National Science Foundation (award OPP-1637708).

Conflict of Interest

None declared.

Submitted 08 February 2019
Revised 19 May 2019
Accepted 16 June 2019

Associate editor: John Melack